JOURNAL OF MATERIALS SCIENCE 30 (1995) 2668–2674

Structural and chemical characteristics and oxidation behaviour of chromium-implanted single crystal silicon carbide

H. DU. Z. YANG, M. LIBERA
Stevens Institute of Technology, Hoboken, NJ 07030, USA
D. C. JACOBSON
AT&T Bell Laboratories, Murray Hill, NJ 07974, USA
Y. C. Wang, R. F. Davis
North Carolina State University, Raleigh, NC 27695, USA

High-dose chromium implantation resulted in complex changes in the structure, chemistry, and oxidation behaviour of beta-type single-crystal silicon carbide. Detailed analytical studies indicated that, in addition to the primary process of surface doping, chromium implantation of silicon carbide to 3.90×10^{17} ions cm^{-2} at 200 keV was accompanied by many secondary processes such as surface sputtering, lattice damaging, and silicon depletion/carbon enrichment in the implanted region. These changes resulted in accelerated oxidation of the implanted samples by a factor of 1.14 as compared with the unimplanted crystals in 1 atm of flowing oxygen at 1100 °C. The oxidation layer exhibited interesting structural and compositional inhomogeneity which could be explained based upon chromium mobility variation in the implanted region. The presence of densely populated chromium oxide precipitates in the outer region of the oxidation layer played a significant role in keeping the degree of oxidation acceleration low under the detrimental influence of lattice damages and silicon deletion/carbon enrichment. It was concluded that the potential of chromium implantation to improve the oxidation resistance of silicon carbide can be realized only when the implantation-induced secondary effects are suppressed.

1. Introduction

Numerous efforts have been made to study the effects of ion implantation on the surface mechanical properties such as wear resistance, hardness, and fracture toughness of advanced ceramics [1–6]. In recent years, there has been an increasing interest in exploring the prospects of ion implantation to improve their surface chemical properties, such as oxidation resistance, with silicon nitride and silicon carbide being the prime targets [7–9].

Ion implantation of ceramics is very complex. In addition to doping, a primary process of implantation, many secondary processes can take place such as surface sputtering, structural alteration, and compositional and phase variations in the implanted region. Particularly, lattice damage and amorphization can readily take place in covalent ceramics [3] in accordance with the temperature ratio and bond-type criteria proposed by Haguib and Kelly [10]. The primary and secondary changes induced by implantation can play opposite roles in the oxidation behaviour of ion-implanted ceramics. As a result, documented oxidation studies of ion-implanted silicon nitride and silicon carbide ceramics have yielded mixed results [7, 8].

Noda *et al.* [7] studied the oxidation behaviour of sintered silicon nitride implanted with chromium to doses in the range 1×10^{17}–5×10^{17} ions cm^{-2} at 200 keV. It was shown that, at temperatures up to 1100 °C, a stable chromia layer was preferentially formed and acted as a good diffusion barrier to inward diffusion of oxygen and outward diffusion of impurity cations present in the sintered specimens. Chromium implantation markedly increased the oxidation resistance of silicon nitride. Above 1100 °C, little difference was observed in the oxidation behaviour between the implanted and unimplanted specimens due to rapid vaporization of chromium oxide.

Based upon the work of Noda *et al.* on silicon nitride [7], ion implantation with chromium should have excellent potential to improve the oxidation resistance of silicon carbide. The studies of McHargue *et al.* [8] resulted in the opposite outcome. It was indicated that chromium implantation to 4×10^{15}–2×10^{16} ions cm^{-2} at 95–280 keV led to accelerated oxidation of hot-pressed and sintered silicon carbide by a factor of up to 1.67 in flowing oxygen at 1300 °C. The decrease in the oxidation resistance was attributed to amorphization of the crystalline specimens in the implanted regions.

0022–2461

The adverse effect of implantation-induced lattice damage on the oxidation resistance was demonstrated in the oxidation studies of self-implanted single-crystal silicon carbide by Du *et al.* [9]. Silicon carbide crystals with residual lattice damage were shown to oxidize 1.16 times faster than unimplanted crystals at 1100 °C. No apparent effect was observed, however, of the lattice damage on the oxidation rate of silicon carbide at 1300 °C due to enhanced damage annealing at relatively high temperatures [9].

McHargue *et al.*'s work [8] illustrated the detrimental structural effect of chromium implantation on the oxidation behaviour of silicon carbide [8]. The chemical effect, i.e. preferential oxidation of chromium to form a chromium oxide barrier layer, could not be determined in their investigation for two reasons. One reason is the relatively low implant dose and the other the relatively high oxidation temperature. It has been shown that high-dose implantation to the order of 10^{16}–10^{18} ions cm^{-2} is often required effectively to improve surface-sensitive properties of ceramics [3] and metals [11]. In the case of oxidation resistance, such dose levels allow the formation of a continuous barrier layer of the implant oxide. On the other hand, even with heavy doses, chromium oxide will no longer be protective above 1100 °C due to its high vapour pressure [7]. Hence an approach which combines high-dose implantation and relatively low oxidation temperature should be pursued to explore the potentially favourable chemical effect of chromium implantation on the oxidation behaviour of silicon carbide. This paper describes the research results in the investigation of the structural and chemical characteristics of single-crystal silicon carbide implanted with chromium to high-dose and the oxidation behaviour of the implanted samples at 1100 °C.

2. Experimental procedure

Sample materials chosen in this investigation were β-type single-crystal silicon carbide (β-SiC) films epitaxially grown on vicinal silicon (1 0 0) using the chemical vapour deposition method described in a review article by Davis and Glass [12]. The as-grown films, approximately 7 μm thick, were microscopically rough and were mechanically polished to a mirror finish using 0.25 μm diamond paste. The samples were ultrasonically cleaned in deionized water, acetone, and methanol to eliminate surface contaminants, and etched in dilute HF solution to remove native oxide prior to implantation.

Chromium implantation of the β-SiC samples was performed at a dose of 3.90×10^{17} ions cm^{-2} at 200 keV. The energetic ions were directed at 7° normal to the sample surface to avoid channelling. The temperature of the samples was maintained at around 550 °C to allow *in situ* dynamic lattice recovery during implantation. Hot implantation has been shown to be an effective means to eliminate implantation-induced amorphization and reduce lattice damage in covalent ceramics [3, 9, 13, 14].

Oxidation experiments of the chromium-implanted β-SiC samples were carried out in 1 atm dry oxygen flowing at 500 standard $cm^3\ min^{-1}$ at 1100 °C for 24 h. Unimplanted samples were also oxidized simultaneously for comparison. The thickness of the oxidation layer on the implanted sample was determined using cross-sectional transmission electron microscopy (XTEM). The thickness of the silica layer formed on the unimplanted sample was measured using an ellipsometer at a wavelength of 632.8 nm.

The chromium-implanted samples before and after oxidation were characterized extensively using various analytical techniques in order to determine the structural and chemical variations which significantly alter the oxidation behaviour. Specifically, Rutherford backscattering spectrometry (RBS) at random and aligned orientations was used to study the implant concentration and the structural changes in the implanted regions. XTEM, selected-area electron diffraction (SAD), and energy dispersive X-ray analysis (EDX) were used to reveal the structural and phase characteristics of the implanted and oxidized samples. Auger electron spectroscopy (AES) and X-ray photoelectron spectroscopy (XPS) were used to determine the elemental distribution and the chemical bonding nature of the elements.

3. Results

3.1. Characteristics of the implanted samples

The structural characteristics of the β-SiC samples used in this investigation as determined by XTEM and RBS were reported elsewhere [9, 12, 14]. In brief, the β-SiC film grown on silicon is a single crystal containing a low density of planar defects. Shown in Fig. 1 are the random and [1 0 0] orientation RBS spectra of the chromium-implanted β-SiC sample obtained using a 2.0 MeV He^+ beam. The close proximity of the random and aligned spectra is indicative of substantially structural and/or chemical changes occurring in the implanted region. The band in the random and aligned spectra around channel number

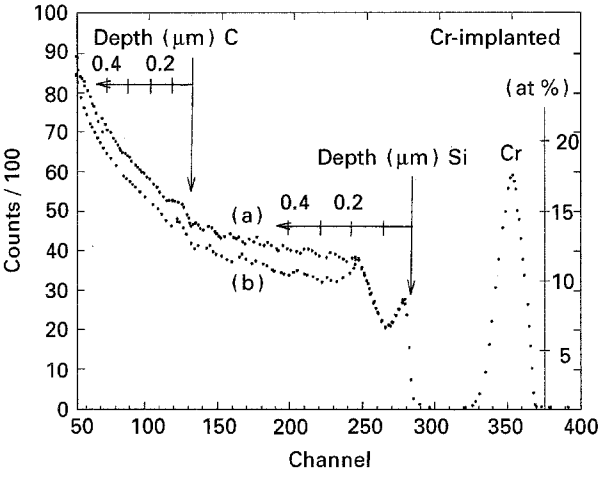

Figure 1 2.0 MeV He^+ RBS spectra of chromium-implanted single-crystal β-SiC at random and [1 0 0] orientation.

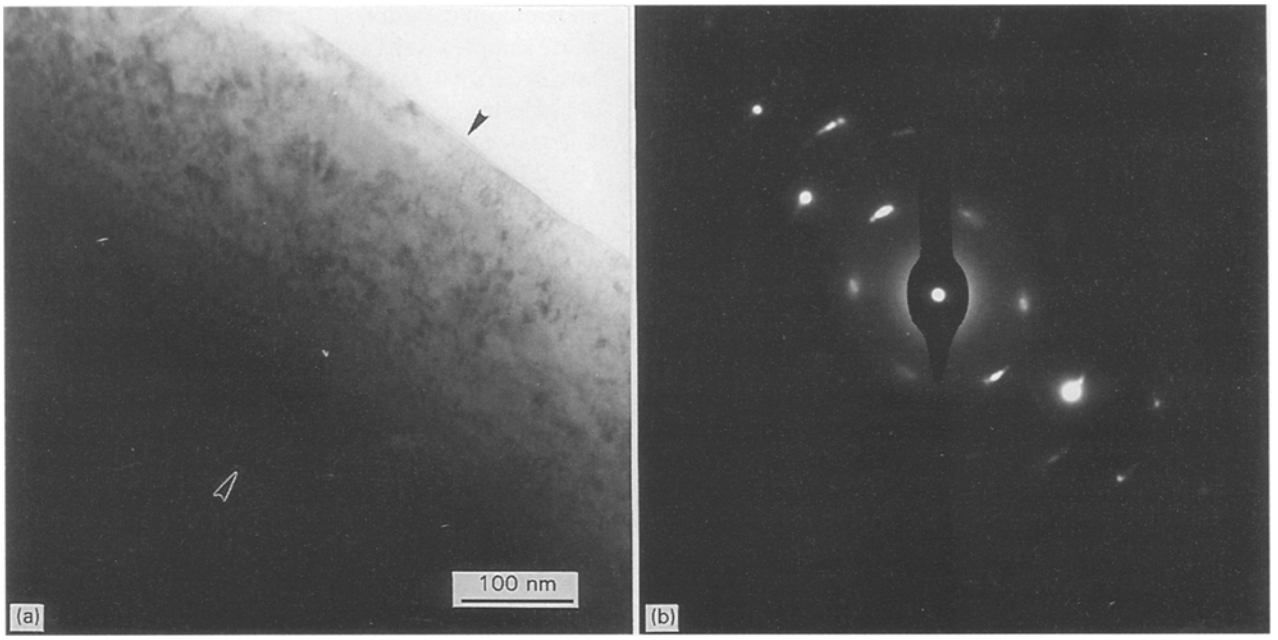

Figure 2 (a) XTEM image, and (b) SAD pattern of chromium-implanted β-SiC along the [1 1 0] zone axis.

350 corresponds to the chromium distribution in the implanted region. The peak chromium atomic concentration is about 18% at approximately 100 nm beneath the sample surface.

Fig. 2a and b depict, respectively, the XTEM image and the SAD pattern of the chromium-implanted sample along the [1 1 0] zone axis. The contrast between the two arrows in Fig. 2a illustrates the structural variations in the implanted region which extends for about 343 nm beneath the sample surface. The asymmetrical feature of the contrast suggests that most of the implantation-induced structural damage and the implant doping occurred in a region closer to the sample surface than to the end-of-damage region. For mono-energy implantation, this asymmetrical nature indicates that sputter removal of the sample surface probably took place during implantation. The SAD pattern in Fig. 2b, which was taken from the high-contrast area approximately 100 nm beneath the implanted sample surface, represents a periodic array of spots characteristic of single-crystal β-SiC. The arcs and broadening in the reflections can be attributed to slight lattice displacement induced by ion implantation. No additional reflections corresponding to other crystalline phases are present.

Fig. 3 shows the AES concentration distribution of the chromium-implanted sample, which was obtained at an electron-beam energy of 3 keV with 5 keV Ar^+ alternating sputtering. The chromium profile was calibrated using the RBS result. The silicon and carbon profiles were plotted with the AES analysis of β-SiC beyond the end-of-damage region as an internal reference. There are two striking features in this figure. First, the chromium distribution in the implanted region is asymmetric. The atomic concentration is approximately 12% at the sample surface. These results offer a direct confirmation of the occurrence of sputtering during chromium implantation, as suggested in the XTEM analysis. Second, the silicon-to-carbon ratio in the implanted region exhibits a varying degree of deviation from the chemical stoichiometry of silicon carbide. Chromium implantation resulted in significant silicon deletion/carbon enrichment in the implanted region.

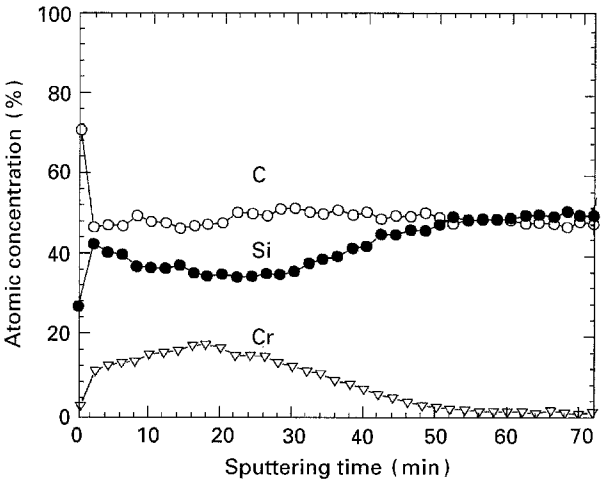

Figure 3 AES elemental concentration distribution in chromium-implanted β-SiC as a function of sputtering time. The sputtering rate is approximately 10 nm min^{-1}.

In addition to structural and compositional variations, ion implantation can also induce the formation of new phases [14]. XPS is an excellent probe for this process owing to its sensitivity to the local chemical environment of an element. Figs 4–6 are the high-resolution XPS spectra of the Cr 2p, Si 2p, and C 1s binding energies collected near the region of peak chromium concentration, respectively. The spectra were taken at a pass energy of 25 eV with MgK_α as the source of excitation. The Cr 2p spectrum in Fig. 4 has a good resemblance to that of chromium metal in peak shape and peak position [15], which indicates

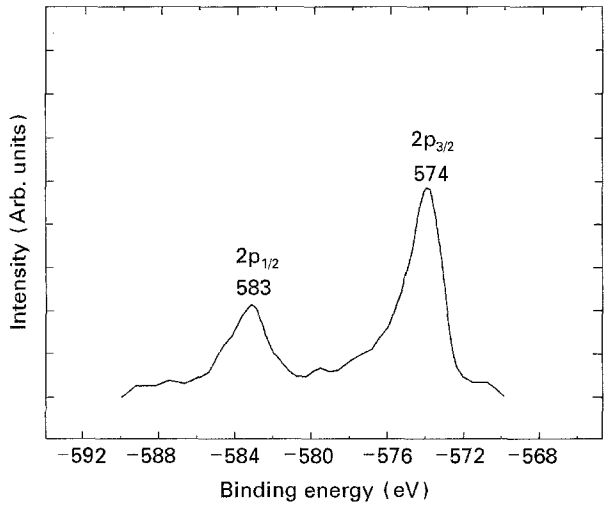

Figure 4 High-resolution XPS spectrum of the Cr 2p binding energy from chromium-implanted β-SiC at around the peak implant concentration.

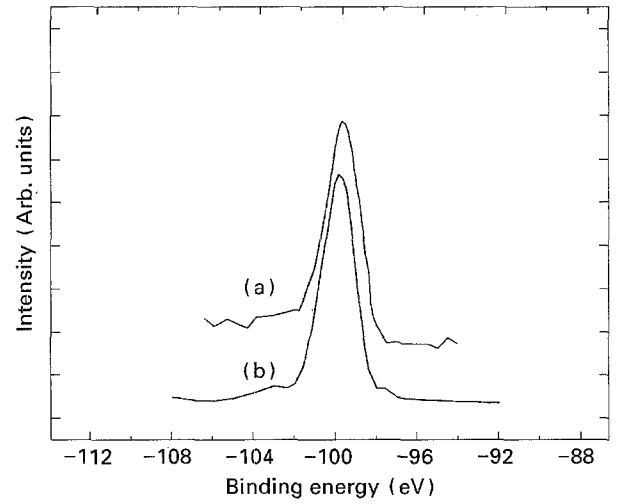

Figure 5 High-resolution XPS spectra of the Si 2p binding energy from (a) chromium-implanted β-SiC at around the peak implant concentration (99.8 eV), and (b) unimplanted β-SiC (100.0 eV).

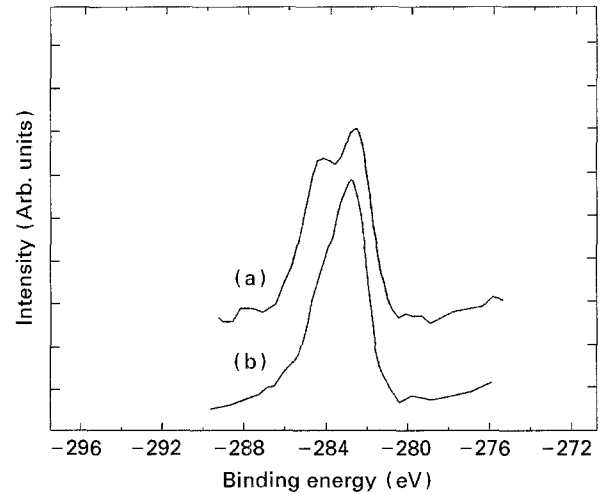

Figure 6 High-resolution XPS spectra of the C 1s binding energy from (a) chromium-implanted β-SiC at around the peak implant concentration (284.6, 282.9 eV), and (b) unimplanted β-SiC (282.9 eV).

that chromium exists in elemental form rather than compound form in the implanted region.

No apparent change occurred in the chemical binding state of silicon during implantation of β-SiC as shown in Fig. 5a and b which depict almost identical Si 2p photoelectron spectra from both the implanted and unimplanted samples. The 0.2 eV shift in the Si 2p binding energy between the two samples probably resulted from the implantation-induced structural modification. In contrast, a significant variation took place in the C 1s spectrum in the implanted region according to Fig. 6. In addition to a C 1s peak component at 282.9 eV, as in silicon carbide, a distinct peak component appeared at around 284.6 eV. This peak component corresponds to that of free carbon [16].

3.2. Oxidation behaviour

Ellipsometry is an ideal technique to measure the thickness of a thin film, uniform in structure and composition. Owing to the expected complexity of the oxidation layer on the implanted sample, XTEM, instead of ellipsometry, was relied upon for accurate thickness determination. Fig. 7 shows an XTEM image of the chromium-implanted sample after oxidation. The inhomogeneity of the oxidation layer is clearly illustrated. The thickness of the oxidation layer is uniform across the oxidized sample surface and is approximately 412 nm based upon the XTEM estimate. In contrast, the thickness of the oxidation layer on the unimplanted sample is only 362 nm according to the ellipsometry measurement.

As depicted in Fig. 7, oxidation of the chromium-implanted sample resulted in the formation of an oxidation layer of non-uniform structure and composition. There exist several regions of different microstructural characteristics and contrast in the oxidation layer. The large grains sparsely and non-uniformly

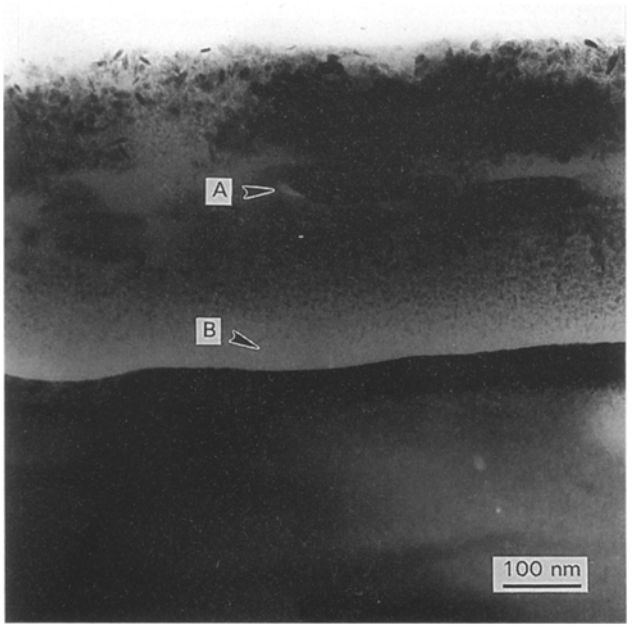

Figure 7 XTEM image of chromium-implanted β-SiC after 24 h oxidation.

distributed in the central portion of the oxidation layer are single-crystal chromium oxide. This is evinced in the SAD pattern shown in Fig. 8a and the EDX spectrum illustrated in Fig. 8b taken from site A in Fig. 7, with an electron probe size of about 10 nm. The smaller but densely populated precipitates in the upper and lower bands of the XTEM image have also been identified to be crystalline chromium oxide. The light region is composed mostly of amorphous silicon dioxide according to the SAD pattern and the EDX spectrum shown, respectively, in Fig. 9a and b taken from site B in Fig. 7. A relatively narrow light band which separates the two bands containing chromium oxide precipitates of dark contrast can also be observed in Fig. 7. This band extends throughout the entire cross-sectional length of the oxidation layer examined and its width does not have any apparent dependence on the presence (or absence) of the large chromium oxide grains. The dark band beneath the oxidation layer in Fig. 7 corresponds to the end of damage region which was not oxidized.

Owing to the charging problem encountered in AES analysis of insulators, XPS was used to study chromium and silicon distribution in the oxidation layer on the chromium-implanted sample at a pass energy of 200 eV. The results are shown in Fig. 10, which depicts the chromium to silicon atomic ratio as a function of sputter time. The two peaks in the profile correspond to two regions with relatively high chromium oxide contents. The area between the two peaks is the region where chromium is depleted. The compositional inhomogeneity in the oxidation layer as revealed by XPS is consistent with the XTEM observations.

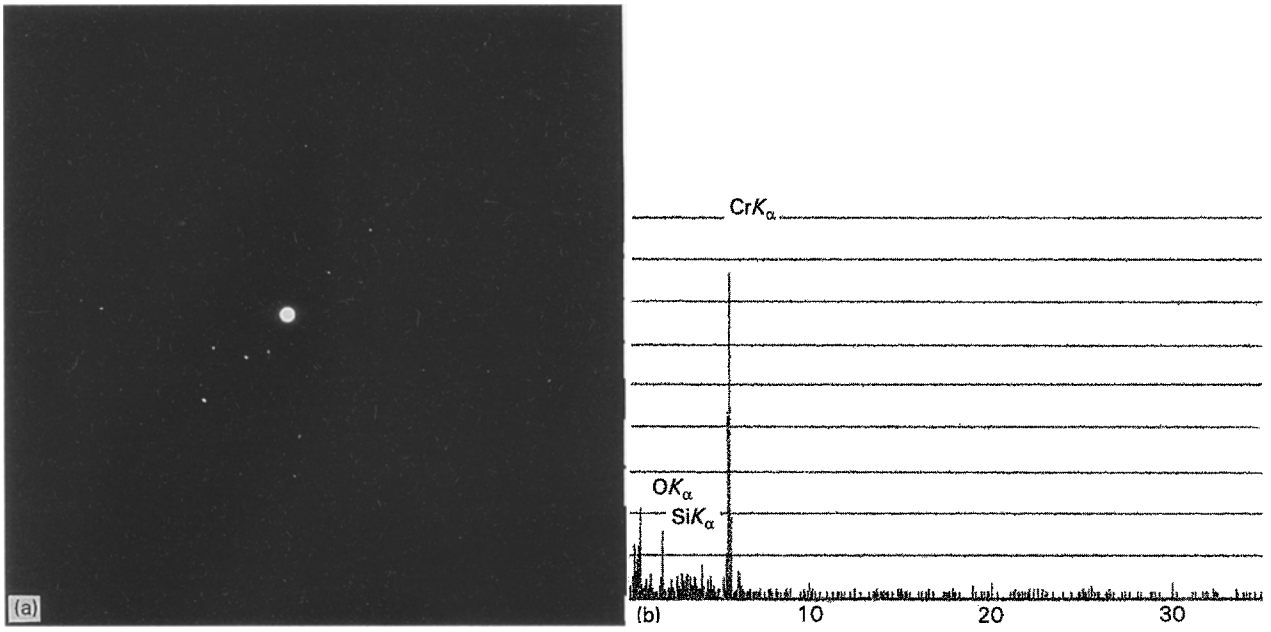

Figure 8 (a) SAD pattern, and (b) EDX spectrum taken from A in Fig. 7.

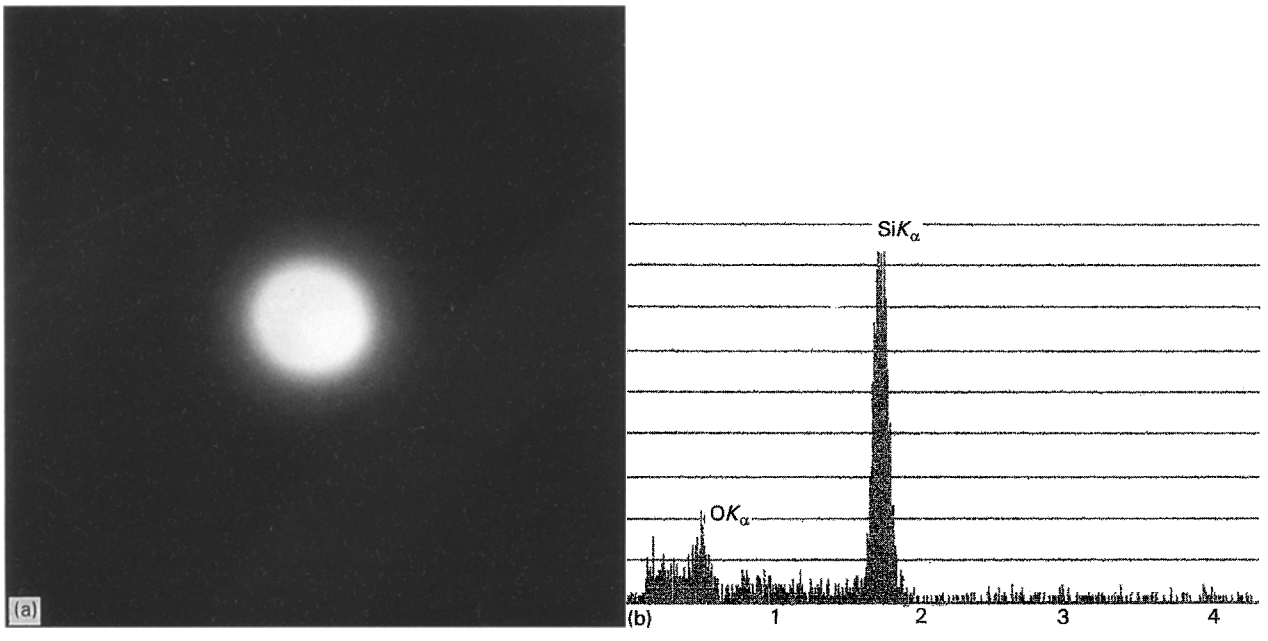

Figure 9 (a) SAD pattern, and (b) EDX spectrum taken from B in Fig. 7.

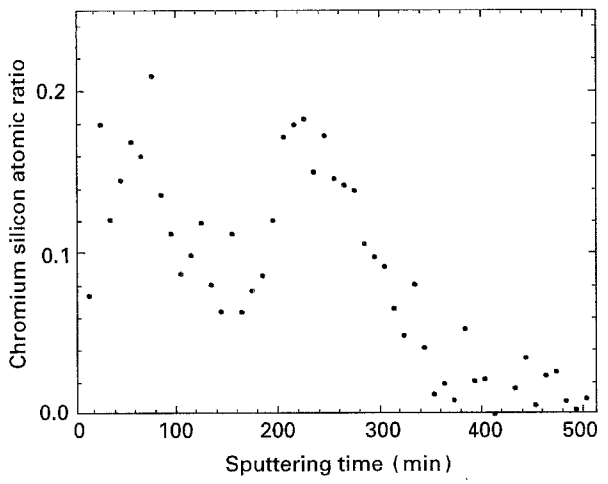

Figure 10 XPS distribution of chromium to silicon atomic ratio in the oxidation layer on chromium-implanted β-SiC as a function of sputtering time. The sputtering rate is approximately 1 nm min^{-1}

4. Discussion

High-dose chromium implantation of β-SiC is very complex. In addition to surface doping with chromium, it is accompanied by various processes such as surface sputtering, lattice displacement, and silicon deletion/carbon enrichment. The structural and chemical variations all contribute to the change in the oxidation behaviour of β-SiC sample implanted with chromium.

Both the XTEM (Fig. 2) and AES (Fig. 3) results strongly suggest that appreciable sputter loss of β-SiC occurred during chromium implantation, although chromium segregation may also contribute to the asymmetry in its concentration distribution. On the one hand, the sputter process reduces the dose level retained in the implanted region. On the other, in the case of mono-energy implantation, this process can help achieve high implant concentration near the surface of the implanted region. A high surface concentration is beneficial, particularly when the chemical effect of the implanted species is to be exploited to improve surface-sensitive chemical properties such as oxidation resistance.

For a given crystalline sample, the structural change induced by ion implantation is a strong function of dose and temperature. White *et al.* [3] noted that at room temperature, a dose as low as 2×10^{14} Cr^{+} cm^{-2} readily amorphized α-SiC crystals, whereas implantation at 750 °C did not produce any amorphous phase. In this investigation, not only did the high-dose implantation at 550 °C effectively eliminate amorphization, it also helped retain the single crystallinity of β-SiC (Fig. 2). These results are indicative of significant *in situ* dynamic annealing and damage recovery during implantation. Such recovery process cannot be attributed to the thermal effect alone, as indicated in the post-implantation studies by Edmond *et al.* [13] who showed that an annealing temperature above 1700 °C is required to recrystallize the amorphized SiC crystals. Hot implantation clearly assisted in the damage recovery via the irradiation-enhancement of the atomic mobility.

The most notable changes induced by chromium implantation are the compositional and phase characteristics. Particularly, the implantation process resulted in significant silicon depletion and carbon enrichment in the implanted region (Fig. 3). The excess carbon existed in the form of free carbon according to the XPS results (Fig. 6). Similar results were reported in the studies of implantation of silicon carbide with high-dose aluminium and nickel [14, 17]. Silicon sublimation and surface graphitization were also shown to occur during vacuum annealing of single-crystal α-SiC above 1000 °C [18]. It is, therefore, reasonable to postulate that the compositional changes observed in this investigation are due to migration of elemental silicon, which resulted from the breaking of the Si–C bond in β-SiC, to the sample surface and subsequent sputter removal and/or sublimation into the vacuum environment during hot implantation. No chromium compounds such as chromium silicide and chromium carbide formed in the implanted region.

The anticipated chemical effect of chromium implantation has not resulted in the enhancement of the oxidation resistance of silicon carbide despite the use of high dose and an oxidation temperature at which chromium oxide is stable. The thickness of the oxidation layer grown on the implanted sample is 1.14 times that of the silica layer on the unimplanted sample after 24 h oxidation. The degree of oxidation acceleration for the chromium-implanted β-SiC is similar to that for the self-implanted β-SiC [9] as compared with unimplanted samples. This result does not necessarily mean that the increase in the oxidation rate of the chromium-implanted sample is due solely to residual lattice damage. In fact, silicon depletion/carbon enrichment will also contribute to rate increase. The chemical effect of chromium incorporation, i.e. formation of chromium oxide diffusion barrier, must have played an important role in keeping the degree of oxidation acceleration low under the combined detrimental effects of the residual lattice damage and the significant change in silicon and carbon composition on oxidation. This argument is consistent with the studies of McHargue *et al.* [8] who showed that, at dose levels where the chemical effect is weak, the degree of oxidation acceleration of chromium-implanted silicon carbide is as high as 1.67.

Thermodynamically speaking, if there is no kinetic constraint, a continuous chromium oxide scale should form at least in the outer region of the oxidation layer particularly when the surface concentration of chromium is high. This is not substantiated in this investigation. As revealed by XTEM (Figs 7–9), the oxidation layer consists of crystalline chromium oxide precipitates embedded in amorphous silicon dioxide. This oxidation characteristic suggests that chromium diffuses through the implanted region less rapidly than oxygen through the oxidation layer towards the oxidation layer–substrate interface. This leads to simultaneous oxidation of chromium and silicon carbide at the reaction interface although preferential oxidation of chromium is thermodynamically favourable.

A striking feature in the characteristics of the oxidation layer formed on the chromium-implanted β-SiC sample is the presence of two regions rich in chromium oxide precipitates which are separated by a narrower region consisting mostly of silica. Studies of the

oxidation layer grown on chromium-implanted silicon nitride by Noda *et al.* [7] also revealed a chromium distribution with two peak concentration regions. The narrow region rich in silica cannot be attributed to the abnormal chromium oxide grain growth because this region is continuous and has no apparent correlation with the distribution of the large chromium oxide grains.

The detailed mechanism is not clear in the evolution of the observed characteristics of the oxidation layer on the chromium-implanted sample. The following postulations can be made, however. In the as-implanted sample, the region around the peak chromium concentration also corresponds to the region with high residual lattice damage. It is expected that the atomic mobility of chromium is much higher in this region than in the region with lower implant concentration. Owing to implantation-induced surface sputtering, the region of high defect and chromium concentrations is near the surface of the implanted sample. During the early period of oxidation, the oxidation layer–substrate interface acts as a diffusion sink to which rapid mass transport of chromium takes place from the region of high chromium concentration and mobility. This process results in the formation of an oxidation layer with a high density of chromium oxide precipitates. Meanwhile, gradual depletion of chromium occurs in the region beneath the reaction interface. This chromium-depleted region is sandwiched by the oxidation layer rich in chromium oxide and an implanted region with relatively low implant concentration and mobility after a certain oxidation period. Subsequent oxidation converts the chromium-depleted region into the silica-rich oxidation layer seen as the narrow band in the XTEM image (Fig. 7).

Further oxidation results in the formation of the remainder of the oxidation layer. The chromium oxide precipitates in the oxidation layer formed during the later period of oxidation have a broader distribution and are less densely populated as compared with the precipitates formed in the earlier oxidation period (Fig. 7). These results are consistent with the speculation that the atomic mobility of chromium is low in the region with relatively low defect and low chromium concentrations. Besides, in a region where the chromium concentration gradient is away from the reaction boundary, long-range diffusion of chromium towards the diffusion sink is not favoured. This should explain the gradual tapering of the population density of the chromium oxide precipitates in the inner oxidation layer towards the oxidation layer–substrate interface. In contrast, the precipitates in the outer oxidation layer are densely accumulated.

5. Conclusion

High-dose ion implantation with chromium resulted in sputter removal as well as complex changes in the structural and chemical characteristics of β-SiC crystals. The implantation process led to lattice damage and, more strikingly, to silicon depletion/carbon enrichment. The excess carbon was present as free carbon in the implanted region. These variations are responsible for the accelerated oxidation of the implanted samples and the formation of the oxidation layer of chemical and structural inhomogeneity. The formation of densely populated chromium oxide in the oxidation outer layer played an important role in reducing the adverse effects of residual lattice damage and the silicon depletion/carbon enrichment on the oxidation resistance of the chromium-implanted samples. However, the favourable chemical effect of chromium implantation was subdued by the secondary effects. To realize the potential of chromium implantation to enhance the oxidation resistance of silicon carbide, the detrimental secondary effects must be minimized.

Acknowledgements

The authors thank Mr J. Ott, ATC/SEM at Stevens, for his assistance in the XTEM analysis and Dr K. T. Shat, AT&T Bell Laboratories, for his assistance in the chromium implantation. A significant portion of the investigation was performed using the ATC/SEM facilities funded by New Jersey Commission on Science and Technology. This work was supported by the National Science Foundation under grant MSS-9110256 and was managed by Dr Jorn Larsen-Basse, Director of the NSF Surface Engineering and Tribology Program.

References

1. J. LANKFORD, W. WEI and R. KOSSOWSKY, *J. Mater. Sci.* **22** (1987) 2069.
2. R. F. HOCHMAN, H. SOLNICK-LEGG and K. O. LEGG, "Ion Implantation and Plasma Assisted Processes", Proceedings of the Conference on Ion Implantation and Plasma Assisted Processes for Industrial Applications, Atlanta, GA, May 1988 (ASM International, Metal Park, OH, 1988).
3. C. W. WHITE, C. J. McHARGUE, P. S. SKLAD, L. A. BOATNER and G. C. FARLOW, in "Materials Science Report" (North-Holland, Amsterdam, 1989) p. 41.
4. N. IWAMOTO, *Trans. Jpn Weld. Res. Inst.* **17** (1988) 85.
5. I. L. SINGER, *Surf. Coatings Technol.* **33** (1987) 387.
6. E. L. FLEISCHER, W. HERTL, T. L. ALFORD, P. BORGESEN and J. W. MAYER, *J. Mater. Res.* **5** (1990) 385.
7. S. NODA, H. DOI, T. HIOKI, J. KAWAMOTO and O. KAMIGAITO, *J. Jpn Soc. Powder Powder Metall.* **35** (1988) 12.
8. C. J. McHARGUE, M. B. LEWIS, J. M. WILLIAMS and B. R. APPLETON, *Mater. Sci. Eng.* **69** (1985) 391.
9. H. DU, M. LIBERA, Z. YANG, P.-J. LAI, D. C. JACOBSON, Y. C. WANG and R. F. DAVIS, *Appl. Phys. Lett.* **62** (1993) 423.
10. H. M. NAGUIB and R. KELLY, *Rad. Effects* **25** (1975) 1.
11. G. DEARNALEY, *Nucl. Instrum. Meth.* **182/283** (1981) 899.
12. F. DAVIS and J. T. GLASS, in "Advances in Solid-State Chemistry", Vol. 2 (JAI Press, London, 1991) p. 111.
13. J. A. EDMOND, R. F. DAVIS and S. P. WITHROW, in "Ceramic Transactions", Vol. 2, Silicon Carbide '87, edited by J. D. Cawley and C. E. Semler (American Ceramic Society, Westerville, OH, 1989) p. 479.
14. H. DU, Z. YANG, M. LIBERA, D. C. JACOBSON, Y. C. WANG and R. F. DAVIS, *Am. Ceram. Soc.* **76** (1993) 330.
15. C. D. WAGNER, W. M. RIGGS, L. E. DAVIS, J. F. MOULDER and G. E. MUILENDERG (eds), "Handbook of X-ray Photoelectron Spectroscopy" (Perkin Elmer Corporation, Eden Prairie, MN, 1979) p. 72.
16. L. PORTE and A. SARTRE, *J. Mater. Sci.* **24** (1989) 271.
17. R. S. BHATTACHARYA, A. K. RAJ and P. P. PRONKO, *J. Appl. Phys.* **61** (1987) 4791.
18. L. MUEHLHOFF, W. J. CHOYKE, M. J. BOZACK and J. T. YATES, Jr, *ibid.* **60** (1986) 2842.

Received 3 December 1993
and accepted 14 November 1994